The EMBO Journal (2006) 25, 4686–4696 | © 2006 European Molecular Biology Organization | All Rights Reserved 0261-4189/06
www.embojournal.org

THE EMBO JOURNAL

A change in conformational dynamics underlies the activation of Eph receptor tyrosine kinases

Silke Wiesner[1,5], Leanne E Wybenga-Groot[2,5], Neil Warner[2,3], Hong Lin[1], Tony Pawson[2,3,*], Julie D Forman-Kay[1,4,*] and Frank Sicheri[2,3,*]

[1]Structural Biology and Biochemistry, Hospital for Sick Children, Toronto, Ontario, Canada, [2]Program in Systems Biology, Samuel Lunenfeld Research Institute, Mount Sinai Hospital, Toronto, Ontario, Canada, [3]Department of Molecular and Medical Genetics, University of Toronto, Toronto, Ontario, Canada and [4]Department of Biochemistry, University of Toronto, Toronto, Ontario, Canada

Eph receptor tyrosine kinases (RTKs) mediate numerous developmental processes. Their activity is regulated by auto-phosphorylation on two tyrosines within the juxta-membrane segment (JMS) immediately N-terminal to the kinase domain (KD). Here, we probe the molecular details of Eph kinase activation through mutational analysis, X-ray crystallography and NMR spectroscopy on auto-inhibited and active EphB2 and EphA4 fragments. We show that a Tyr750Ala gain-of-function mutation in the KD and JMS phosphorylation independently induce disorder of the JMS and its dissociation from the KD. Our X-ray analyses demonstrate that this occurs without major conformational changes to the KD and with only partial ordering of the KD activation segment. However, conformational exchange for helix αC in the N-terminal KD lobe and for the activation segment, coupled with increased inter-lobe dynamics, is observed upon kinase activation in our NMR analyses. Overall, our results suggest that a change in inter-lobe dynamics and the sampling of catalytically competent conformations for helix αC and the activation segment rather than a transition to a static active conformation underlies Eph RTK activation.

The EMBO Journal (2006) **25,** 4686–4696. doi:10.1038/sj.emboj.7601315; Published online 14 September 2006
Subject Categories: signal transduction; structural biology
Keywords: activation mechanism; crystal structure; Eph receptor tyrosine kinase; NMR spectroscopy

*Corresponding authors. F Sicheri, Samuel Lunenfeld Research Institute, Mount Sinai Hospital, 600 University Ave., Toronto, Ontario, Canada M5G 1X5. Tel.: +1 416 586 8471; Fax: +1 416 586 8869; E-mail: sicheri@mshri.on.ca or JD Forman-Kay, Hospital for Sick Children, 555 University Ave., Toronto, Ontario, Canada M5G 1X8. Tel.: +1 416 813 5358; Fax: +1 416 813 5022; E-mail: forman@sickkids.ca or T Pawson, Samuel Lunenfeld Research Institute, Mount Sinai Hospital, 600 University Ave., Toronto, Ontario, Canada M5G 1X5. Tel.: +1 416 586 8262; Fax: +1 416 586 8869; E-mail: pawson@mshri.on.ca
[5]These authors contributed equally to this work

Received: 21 April 2006; accepted: 8 August 2006; published online: 14 September 2006

Introduction

Eph receptors regulate numerous developmental and cellular processes such as cell attraction/repulsion, adhesion/detachment and migration, thereby influencing morphogenesis and organogenesis (Kullander and Klein, 2002). The Eph receptor tyrosine kinase (RTK) family is divided into two groups, A and B, based on sequence similarity and a preference for binding to their ligands, the A- and B-type ephrins, respectively (Eph Nomenclature Committee, 1997). The domain structure of Eph RTKs is highly conserved from worm to human and consists of an extracellular N-terminal ligand-binding domain, a cysteine-rich region, two fibronectin type III repeats, a single membrane-spanning segment, a juxta-membrane segment (JMS), a tyrosine kinase domain (KD), a SAM domain and a C-terminal PDZ domain binding motif. Binding of ephrins to the extracellular domain of the Eph receptors leads to receptor multimerization and the activation of the cytoplasmic KD. Catalytic activation correlates with auto-phosphorylation on two tyrosines (Tyr604 and Tyr610, for murine EphB2) within the JMS (Ellis *et al*, 1996; Zisch *et al*, 1998; Binns *et al*, 2000) and possibly on a conserved residue, Tyr788, within the KD activation segment (referred to herein as Y^{act}). In the absence of phosphorylation, the JMS represses the catalytic function of the adjacent KD through an intramolecular mechanism (Binns *et al*, 2000; Wybenga-Groot *et al*, 2001).

The crystal structure of an unphosphorylated EphB2 fragment comprised of the JMS and the KD (EphB2 JMS-KD) revealed an auto-inhibitory state, in which an ordered α-helical JMS intimately associates with the KD (Wybenga-Groot *et al*, 2001). The majority of JMS contacts were directed at the N-lobe of the KD centered on helix αC and the adjacent β4-strand. Interestingly, helix αC possessed a kink not previously observed in active state protein kinase structures. In addition, more limited JMS contacts with the KD C-lobe appeared to prevent the activation segment from adopting an ordered productive conformation. Lastly, the JMS bridged the N- and C-lobes of the KD and thereby seemed to restrict inter-lobe flexibility. Together, these disruptive features were proposed to account for the repressed catalytic function of Eph receptors in their auto-inhibited states.

Based on comparisons with the active insulin RTK structure (Hubbard, 1997) and structure-based mutational analyses, a two-component mechanism of catalytic activation was proposed for the Eph receptor family whereby phosphorylation of Tyr604 and Tyr610 within the JMS would cause the dissociation of the JMS from the KD (Wybenga-Groot *et al*, 2001). This event would relieve the distortion to helix αC and steric effects preventing the ordering of the activation segment. The latter, possibly supported by phosphorylation of Y^{act}, would then allow the activation segment to adopt a productive conformation. However, a more recent crystal structure of a non-phosphorylated fragment of EphA2 containing exclusively the KD revealed a kinked helix αC and a

significantly disordered activation segment (Nowakowski *et al*, 2002). Nevertheless, the EphA2 crystallization construct displayed robust catalytic activity in solution. These results have led us to experimentally revisit the mechanisms by which Eph RTKs are regulated.

Here, we extend our analysis of the Eph receptor catalytic switching mechanism through a combination of mutational analyses, crystal structures and NMR studies of multiple EphB2 and EphA4 receptor proteins corresponding to auto-inhibited and active states. Using NMR spectroscopy, we provide direct evidence that phosphorylation of the JMS residues Tyr604 and Tyr610 induces disorder of the JMS and its dissociation from the KD. Our X-ray analyses show that JMS dissociation occurs without major structural changes to helix αC in the KD, but with partial ordering of the activation segment. Furthermore, NMR studies provide conclusive evidence that kinase activation coincides with increased inter-lobe flexibility and that helix αC samples conformations in solution that deviate from the kinked conformation observed in the crystal structures. In light of these data, we propose a refined model for Eph receptor regulation that suggests new avenues for further research.

Results

Mutational analysis of Tyr750

In the catalytically repressed EphB2 crystal structure, the C-lobe residue Tyr750 lies in direct vicinity to the JMS at the inter-lobe cleft and physically prevents the activation segment from adopting a productive conformation (Wybenga-Groot *et al*, 2001). Furthermore, Tyr750 in EphB2 is detectably phosphorylated *in vivo* and, therefore, could serve a phosphoregulatory function (Kalo and Pasquale, 1999). To specifically investigate the functional importance of Tyr750 in Eph receptor regulation, we first mutated this residue to Phe in an EphA4 JMS-KD receptor fragment (Figure 1A). For clarity, we employ EphB2 numbering with the corresponding EphA4 numbering in parentheses (the JMS-KD of EphA4 and EphB2 share 84% sequence identity). If phosphorylation of Tyr750 (Tyr742) was required for full activation, it would be expected that a Tyr750Phe mutant would be less active than wild-type EphA4 JMS-KD, whereas a Tyr750Glu mutant (mimicking phosphorylation at this position) would restore activity to a JMS-KD protein that is constitutively repressed by an additional Tyr604/610Phe (Tyr596/602Phe) double mutation. The latter substitutions were previously shown to completely repress catalytic function both *in vitro* and *in vivo* by preventing auto-phosphorylation on the JMS regulatory sites (Wybenga-Groot *et al*, 2001). The two purified EphA4 mutant proteins were tested for their ability to auto-phosphorylate (Figure 1A), to phosphorylate enolase (data not shown) and to phosphorylate a peptide substrate in a continuous spectrophotometric assay (Figure 1B). The EphA4 Tyr604/610Phe double mutant and wild-type JMS-KD proteins were analyzed concomitantly as reference points for the repressed (non-activatable) and

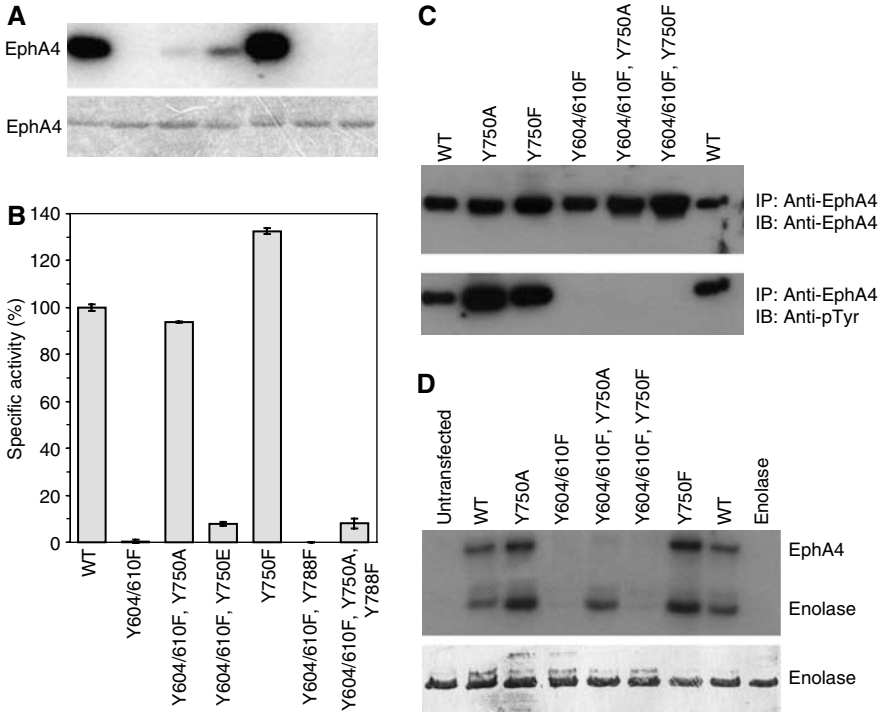

Figure 1 The Tyr750Ala mutation increases Eph RTK activity. (**A**) Purified EphA4 proteins were assessed for their ability to auto-phosphorylate in an *in vitro* kinase assay (top panel). Coomassie-stained SDS–PAGE analysis (lower panel) shows that equal quantities of EphA4 proteins were employed in each kinase reaction. Lanes labeled as in (B). (**B**) Histogram of the specific activities of purified EphA4 proteins measured by the spectrophotometric coupling assay at 0.5 mM S1 peptide and 0.5 μM EphA4 kinase protein. Velocities were normalized to the specific activity of wild-type EphA4 (top panel). (**C**) Full-length EphA4 wild-type and mutant receptors were expressed in COS-1 cells and immunoprecipitated. The immunoprecipitates were resolved by SDS–PAGE and immunoblotted with anti-EphA4 (top panel) or anti-phospho tyrosine (lower panel). (**D**) EphA4 immunoprecipitates were assessed for their ability to auto-phosphorylate and phosphorylate enolase by an *in vitro* kinase assay (top panel). Coomassie-stained SDS–PAGE analysis (lower panel) shows that equal quantities of enolase were employed in each kinase reaction.

active (fully activatable) states, respectively. A schematic of all Eph receptor constructs used in this study is shown in Supplementary Figure S1.

Mutation of Tyr750 to Phe in the wild-type JMS-KD background did not adversely affect EphA4 kinase activity (Figure 1A and B, lanes 1 and 5). This suggests that Tyr750 is not a phosphoregulatory site or that, minimally, phosphorylation of Tyr750 is not essential for the catalytic activation of EphA4 JMS-KD *in vitro*. Mutation of Tyr750 to Glu in the repressed JMS background (Tyr604/610Phe) did not robustly rescue catalytic function in either kinase assay (Figure 1A and B, lane 4) and the same mutation in the wild-type background did not increase catalytic function (Supplementary Figure S2). These results further suggest that Tyr750 does not serve an essential phosphoregulatory function. In contrast to the Tyr750Glu mutant, a Tyr750Ala mutation fully rescued catalytic function of the constitutively repressed Tyr604/610Phe mutant to wild-type levels (Figure 1B, lane 3). As two prominent auto-phosphorylation sites have been removed from this protein ($Y^{604/610}$), the level of auto-phosphorylation was expected to decrease relative to its wild-type counterpart (Figure 1A, lane 3). Accordingly, the near absence of phospho-tyrosine incorporation into all Tyr604/610Phe mutants (Figure 1A, lanes 2, 3, 4, 6 and 7) suggests that sites other than Tyr604 and Tyr610 (most importantly, Y^{act} in the activation segment) are not significant targets for auto-phosphorylation *in vitro*. Supporting this notion, we find that the EphA4 JMS-KD fragment efficiently phosphorylates short peptides encompassing the JMS tyrosines 604 and 610 but not peptides containing the conserved tyrosine 750 and tyrosine 788 (Y^{act}) of EphA2, EphA4 and EphB2 receptors (Supplementary Figure S3). Overall, our results indicate that a bulky side chain at position 750 is required for the repression of catalytic function by an unphosphorylated JMS.

To test whether these *in vitro* results are relevant to the full-length receptor *in vivo*, we introduced Tyr750 mutations into full-length EphA4 receptor and investigated the properties of these mutants by transient transfection in COS-1 cells (Figure 1C and D). Overexpression of wild-type Eph RTKs in such cells yields constitutive auto-phosphorylation on $Y^{604/610}$ and, hence, receptor activation without a need for ephrin stimulation. EphA4 variants were immunoprecipitated and then analyzed for auto-phosphorylation activity and phosphorylation of enolase substrate (Figure 2C and D). Mutation of Tyr750 to either Ala or Phe in an otherwise wild-type receptor did not perturb catalytic function as compared to wild-type EphA4 (Figure 1C, lanes 1–3). Consistent with the *in vitro* results, mutation of Tyr750 to Ala in the fully repressed (Tyr604/610Phe) full-length EphA4 produced a highly active receptor, as indicated by the extent of enolase phosphorylation (Figure 1D, lane 5). As observed for the JMS-KD fragment, the auto-phosphorylation level for this mutant was virtually undetectable (Figure 1C, lane 5). Again, these observations suggest that the activation segment is not a significant auto-phosphorylation site *in vitro* or *in vivo*. In contrast, mutation of Tyr750 to Phe in the repressed (Tyr604/610Phe) JMS background did not rescue catalytic activity (Figure 1D, lane 6). Similar results were obtained for full-length variants of the EphB2 receptor transiently transfected into 293T cells (data not shown). These findings support a role for Tyr750 in either composing the binding site for the JMS and/or in physically blocking the ordering of the activation segment in response to the binding of the JMS to the KD.

Crystallographic analyses of active forms of EphB2 and EphA4

Despite the absence of the JMS, the crystal structure of the isolated EphA2 KD displays great similarity to the auto-inhibited EphB2 JMS-KD structure (Nowakowski *et al*, 2002). In particular, helix αC remains kinked and much of the activation segment is disordered. To investigate whether the active EphA2 KD structure is representative of other Eph receptor active states, we crystallized the isolated KD of EphB2 (aa 622–906) and an EphA4 JMS-KD fragment, bearing the kinase-repressing Tyr604/610Phe double mutation, but activated by a Tyr750Ala mutation (described above) (Supplementary Figure S1), and determined their X-ray structures by molecular replacement (see Supplementary data for details). A summary of the data collection and refinement statistics is given in Table I. As expression of catalytically active variants of EphB2 (but not EphA4) is toxic to bacteria, we introduced a kinase inactivating Asp754Ala mutation far removed from the JMS binding site in all EphB2 crystallization and NMR constructs described herein (Supplementary Figure S1). This mutation of the putative catalytic base (Hanks and Hunter, 1995) is predicted to inactivate the kinase without perturbing the structure of the KD itself.

In brief, the refined EphB2 KD crystallographic model consists of four KD molecules in the asymmetric unit (referred to as molecules A–D), each with one ADP molecule and one magnesium ion bound. This model was refined to 2.6 Å to an R_{factor}/R_{free} 20.4%/26.1% (Table I). The four EphB2 KD structures are well ordered, except for five C-terminal residues and residues 774–796 corresponding to the kinase activation segment. The EphA4 Tyr604/610Phe, Tyr750Ala JMS-KD fragment, which contains one molecule in the asymmetric unit, was refined to 2.35 Å to an R_{factor}/R_{free} of 20.9/24.8% (Table I). Overall, the KD in the EphA4 structure is well ordered, with the exception of residues 651–654 (642–646) connecting β-strands 2 and 3, residues 665 and 666 (657–658) connecting strand β3 and helix αC, residues 779–794 (771–784) of the activation segment and eight C-terminal residues. Most notably, the JMS (599–621 in EphB2; 591–613) is almost completely disordered in this model, suggesting that the Tyr750Ala mutation restores catalytic function at least in part by directly perturbing the JMS–KD interaction.

Overview of the active state Eph structures. The active state KD structures of EphA4, EphB2 and for comparison EphA2 (with two molecules in the asymmetric unit denoted A and B, PDB ID 1MQB) (Nowakowski *et al*, 2002) adopt canonical bilobal folds (Figure 2A). The N-lobe consists of a twisted five-strand anti-parallel β-sheet and a single helix αC, whereas the C-lobe is predominantly α-helical. The N- and C-lobes are connected by a short linker termed the hinge. Flexibility about the hinge is known to allow for a range of conformations, with the catalytically competent conformation typically corresponding to a closed conformation (Huse and Kuriyan, 2002). Comparison of the KDs in the EphA4 Y604/610F, Y750A JMS-KD and EphB2 KD structures reveals a greater

Table I Data collection, structure determination and refinement statistics for active Eph receptor KD structures

	EphB2 D754A KD (ADP)	EphA4 Y604/610F, Y750A JMS-KD
Wavelength	$\lambda = 1.54180$ Å	$\lambda = 1.54180$ Å
Space group	$P2_1$	$P2_1$
Resolution (Å)	2.6	2.35
Reflections, total/unique	428 269/41 270	26 864/9232
Completeness (%)[a]	99.8 (99.5)	88.6 (54.9)
R_{sym} (%)[a,b]	8.2 (24.9)	5.7 (12.8)
$\langle I/\sigma \rangle$[a]	16.9 (4.3)	17.2 (4.5)
Refinement		
Resolution range (Å)	24–2.6	30–2.35
Reflections		
All data	40 244	9085
$\|F\| > 2\sigma$	37 259	8467
R_{factor}/R_{free} (%)[c]		
All data	20.4/26.1	20.9/24.8
$\|F\| > 2\sigma$	19.4/25.2	20.0/23.9
Residues in disallowed/most favored regions of the Ramachandran plot	0/88.0%	0.9/86.8%
Average *B*-value (Å^2)	31.6	42.4
RMSD for main-chain *B*-values (Å^2)	0.98	1.00
RMSD for side-chain *B*-values (Å^2)	1.59	1.54
RMSD for bonds (Å)	0.008	0.006
RMSD for angles (deg)	1.09	0.96
Number of non-hydrogen protein atoms	8155	1968
Number of non-hydrogen nucleotide atoms	108	—
Number of water molecules	301 (+4 Mg^{2+})	51

[a]Numbers given in parentheses refer to data for the highest resolution shell.
[b]$R_{sym} = 100 \times \sum|I - \langle I \rangle| / \sum \langle I \rangle$, where I is the observed intensity and $\langle I \rangle$ is the average intensity from multiple observations of symmetry-related reflections.
[c]R_{free} value was calculated with 10% of the data for EphB2 D754A KD, and 6% of the data for EphA4 Y604/610F, 750A JMS-KD.

degree of variability in lobe closure for the active state structures than displayed by the two unique molecules in the auto-inhibited EphB2 JMS-KD crystal structure (denoted A and B, PDB ID 1JPA) (Figure 2A and Supplementary Table SI). Although the degree of lobe closure for each active state structure is influenced in part by crystal packing interactions (as evidenced by differences between EphB2 KD molecules A–D) and the presence (EphB2) or absence (EphA4 and EphA2) of bound nucleotide, it is also conceivable that the greater range of lobe closures for the active state structures reflects an absence of the JMS, which by bridging both catalytic lobes would restrict inter-lobe flexibility. With the exception of the JMS and the activation segment, no gross conformational changes are observed in the N- or C-lobe of the KDs relative to the auto-inhibited EphB2 crystal structure (Figure 2A). However, the N-lobe appears to be slightly more affected than the C-lobe by the attainment of an active state as evidenced by a greater average RMSD between active and inactive state structures for the N-lobe (0.54 Å^2) than for the C-lobe (0.33 Å^2) (Supplementary Table SI). This is attributable to small differences in the relative position of helix αC with respect to the adjacent β-sheet of the N-lobe (Figure 2A).

An increase in inter-lobe flexibility for the active state EphB2 structures relative to the auto-inhibited EphB2 structures gives rise to a binding mode for the nucleotide that is more consistent with catalytic activity. In contrast to the auto-inhibited EphB2 structures (Figure 2), which were characterized by the presence of an ordered adenine base and complete disorder of the sugar and phosphate groups of the non-hydrolyzable ATP analogue AMP-PNP, the entire bound ADP molecule is ordered in all four EphB2 active state structures (Supplementary Figure S4). This change in nucleotide binding arises from an increase in lobe closure, which effectively translates the G-loop and invariant Lys–Glu salt bridge (between subdomains II and III) 2.4 Å (±0.3 Å) and 1 Å (±0.3 Å) toward the C-lobe.

Although ATP binding appears more productive in the active state EphB2, two features differentiate the KD structure from prototypical active state conformations (such as that observed for PKA). Firstly, a kink in the N-lobe helix αC, previously attributed to the Eph receptor auto-inhibited state, persists in all seven active state structures (Figure 2B). In addition, the peptide substrate docking site, comprising the C-terminal portion of the activation segment, is disordered in all seven active state structures. A kinked helix αC and disordered activation segment are not likely catalytically competent conformations but may be dominant conformations (enthalpically favorable) in solution for the 'active state,' with catalysis occurring upon transient sampling of unkinked αC and ordered activation segments (see below).

Role of Tyr750 in activation segment conformation. Disorder of the activation segment is a common feature of many inactive and far fewer active kinase state structures (Nolen *et al*, 2004). Figure 2C displays a superposition of the activation segment region of all active and auto-inhibited Eph receptor KD structures. Interestingly, although the majority of the activation segment is disordered for all structures, the extent of disorder is reduced in all the active state structures relative to auto-inhibited state structures. An increase in the order is observed for one to seven N-terminal and up to two C-terminal residues of the active state activation segments (Supplementary Table SI). The more extensive ordering of the activation segment of EphA2 molecule B correlates with a change in the Tyr750 side chain rotamer that allows for a productive path of the activation segment (Figure 2D). Importantly, the ability of Tyr750 to adopt a non-impeding rotamer is dependent on the dissociation of the JMS from the KD, as the Tyr750 side chain and the JMS would otherwise occupy the same physical space. In the only other active state structure with extensive ordering of the activation segment, the EphA4 Y604/610F, Y750A JMS-KD fragment, the bulky Tyr side chain of position 750 is entirely absent owing to its substitution by Ala. The correlation of Tyr750 position with more extensive ordering of the activation segment lends support to a role for Tyr750 in modulating activation segment conformation in response to JMS dissociation from the KD.

In summary, our crystallographic analyses of Eph active state structures reveal evidence of an increase in inter-lobe flexibility, a partial ordering of the activation segment and the maintenance of a fully kinked helix αC. Subtle structural plasticity in the position of helix αC with respect to the N-lobe β-sheet structure is also apparent, which together may account for the enhanced catalytic function of our active state EphB2 protein constructs.

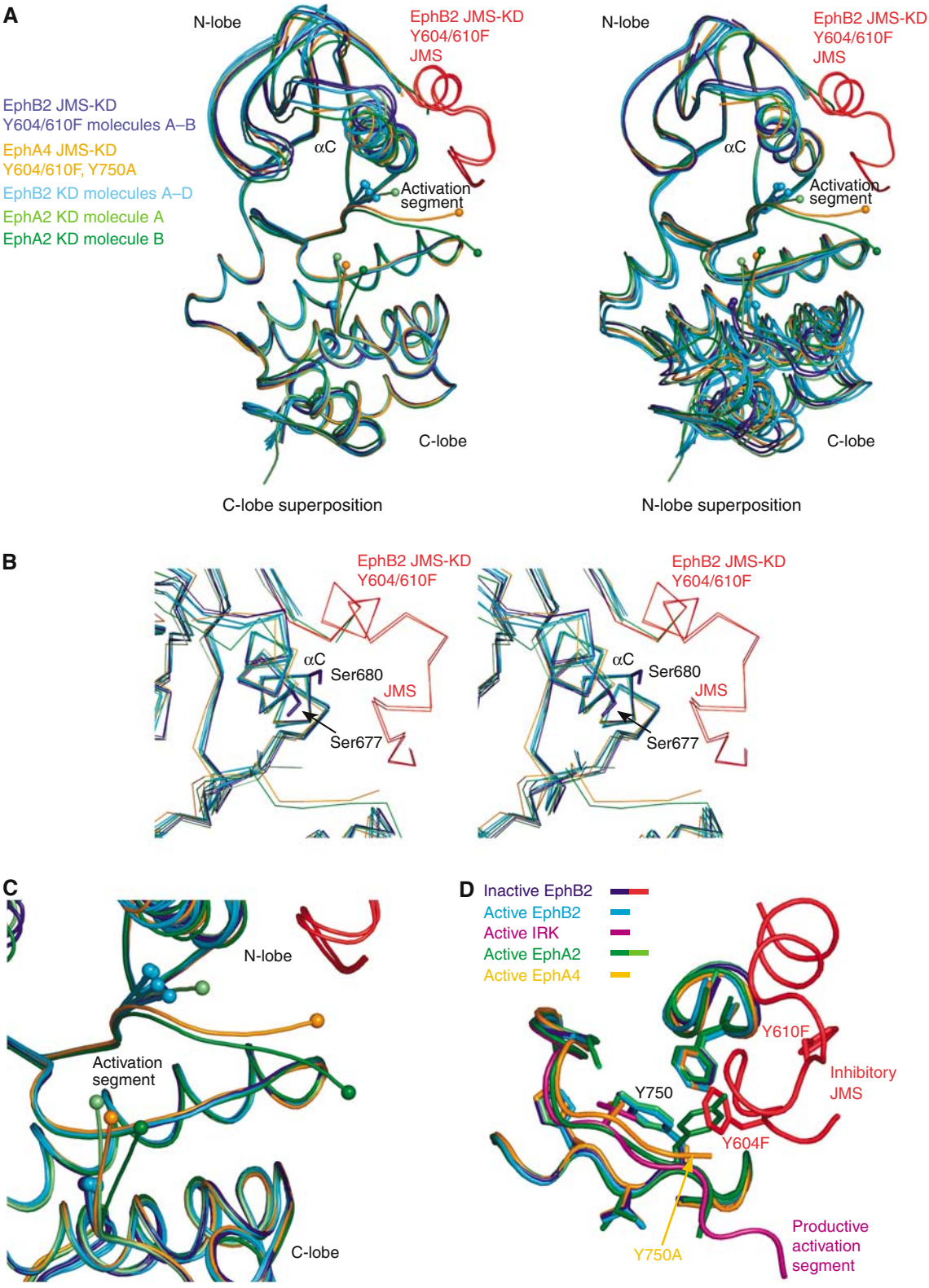

Figure 2 Comparison of Eph receptor KD crystal structures. (**A**) Superposition of active Eph KD structures with auto-inhibited EphB2 structures (PDB ID 1JPA). KDs were aligned using C^{α} atoms of the C-lobes (left panel) and C^{α} atoms of the N-lobes (right panel). Spheres represent the ordered boundaries of the KD activation segment. (**B**) Stereo view of kinked KD helices αC. The Eph receptor KDs (colored as in panel A) were superimposed using C^{α} atoms of helix αC. The kink stabilizing side chains of Ser677 and Ser680 in auto-inhibited EphB2 JMS-KD are shown in dark blue. (**C**) View of the inter-lobe cleft, highlighting the ordered regions of the KD activation segments (colored as in panel A). (**D**) Superposition of EphB2 JMS-KD with the active Eph KD structures, highlighting the region surrounding Tyr750. Backbone traces are colored as in panel A, with all side chains colored according to their respective backbones. The backbone of a typical activation segment conformation from the active insulin RTK (1IR3) is shown in magenta.

NMR studies of inhibited and activated forms of EphB2

Eph receptor activation is hypothesized to involve a transition of the JMS from an ordered KD-associated state to a disordered state. We applied NMR spectroscopy to further investigate this issue, as changes in protein conformation and dynamics are readily identified by changes in the amide resonances in $^{1}H,^{15}N$-correlation (HSQC) spectra. In order to localize regions involved in conformational change in an HSQC analysis (i.e. a chemical shift perturbation study), a full assignment of protein kinase amide resonances in at least one functional state (auto-inhibited or active) is required. To enable NMR studies of the Eph RTK system, we identified conditions under which an unphosphorylated and thus auto-inhibited EphB2 JMS-KD fragment could be expressed and refolded in sufficient quantities (see Supplementary data for details). This construct then served as a point of reference for the analysis of active state models described below.

Characterization of the auto-inhibited EphB2 JMS-KD Fragment. A $^{2}H,^{13}C,^{15}N$-labeled protein sample of auto-inhibited EphB2 JMS-KD was prepared and more than 90% of all $^{1}H^{N},^{13}C,^{15}N$ backbone resonances were assigned using relaxation-optimized (TROSY) heteronuclear NMR experiments. No resonance assignments could be obtained for the first five residues of the expression construct, residues 652, 666 and 724 in loop regions, the N-terminal half of the activation segment (aa 772–782) and three residues that follow proline residues (aa 798, 835 and 861). As the inability to assign many of these residues likely reflects conformational dynamics, it is worth noting that the N-terminal region of the JMS, the β2/β3-loop containing Gly652 and the entire activation segment were disordered in the auto-inhibited EphB2 crystal structure (Wybenga-Groot *et al*, 2001). Although we could assign the C-terminal half (aa 783–796) of the activation segment, reduced signal intensities, random coil $^{13}C^{\alpha}$ and $^{13}C^{\beta}$ chemical shifts (Supplementary Figure S5A) and ^{15}N relaxation properties (unpublished results) indicate substantial disorder for these residues, which again is in agreement with the auto-inhibited EphB2 crystal structure.

Overall, comparison of the assigned $^{13}C^{\alpha}$ and $^{13}C^{\beta}$ resonances with random coil values (secondary chemical shifts) (Supplementary Figure S5A) shows that the secondary structure of the auto-inhibited EphB2 JMS-KD in solution is very similar (if not identical) to that observed for the crystal structure. Importantly, in the absence of phosphorylation, the JMS adopts a stable α-helical conformation in solution. This observation also demonstrates that the employed Asp754Ala kinase-inactivating mutation is non-perturbing to KD structure.

Analysis of EphB2 'activated state' constructs. In order to map structural changes that arise in response to kinase activation, we characterized $^{1}H,^{15}N$-correlation spectra of three different EphB2 constructs, each reflective of an active state attained by different means. These constructs included (1) the isolated EphB2 KD, which is free of all inhibitory influence from the JMS (Wybenga-Groot *et al*, 2001), (2) an EphB2 JMS-KD fragment phosphorylated on the JMS tyrosines 604 and 610 (EphB2 pY604/610 JMS-KD; this is most representative of the natural basis for receptor activation) and (3) the EphB2 JMS-KD fragment containing a Tyr750Ala mutation (Supplementary Figure S1).

As shown in Figure 3A, C and E, all three active state spectra are characterized by large chemical shift changes and/or increased line broadening relative to the auto-inhibited Eph receptor spectrum. In order to visualize regions of the EphB2 proteins that are most affected by transition to an active state, spectral changes were quantified by dividing peak intensities in the active state spectra with those in the auto-inhibited reference spectrum (this approach requires resonance assignments for only one kinase state). Peak intensities were measured at the precise position of the assigned peak in the auto-inhibited EphB2 spectrum. As our point of reference is the auto-inhibited state, significant movement of a resonance peak or its complete broadening in the active state spectra is not distinguishable and, hence, was scored in the same way (i.e. as a relative peak intensity of zero). The resulting relative peak intensities were mapped onto the crystal structure of auto-inhibited EphB2 JMS-KD (Figure 3B, D and F). Surprisingly, although the three constructs were activated by different means, the residues most affected by activation are strikingly similar (Supplementary Figure S6).

The active state EphB2 KD. The $^{1}H,^{15}N$-correlation spectrum of EphB2 KD is markedly different from that of the auto-inhibited EphB2 JMS-KD (Figure 3A). The most notable difference is the loss of resonances attributable to the JMS (aa 598–621) that is absent from the EphB2 KD construct (Supplementary Figure S1). Furthermore, significant spectral perturbations were observed for almost the entire N-lobe of the KD, the hinge and regions within the C-lobe that face the inter-lobe cleft, such as the activation segment and the catalytic loop (Figure 3A and B and Supplementary Figure S6). Resonances of residues in helix αC, strand β4 and the N-terminal half of the catalytic loop encompassing the important Tyr750 site were expected to be strongly perturbed for the isolated KD, as these regions constitute the contact site for the JMS in the auto-inhibited structure (Supplementary Figure S6). However, the large spectral perturbations for residues in the G-loop, the C-terminal half of strand β3, the hinge, the C-terminal half of the catalytic loop, strand β8 and the C-terminal half of the activation segment cannot be accounted for simply due to a loss of contact to the JMS, as these regions of the KD are spatially remote from the JMS binding site (Figure 3A and Supplementary Figure S6). Therefore, we interpret these chemical shift perturbations as reflecting allosteric (i.e. remote) changes in conformation or a change in protein dynamics.

The Tyr604 and Tyr610 phosphorylated EphB2 JMS-KD. For our second active state NMR analysis, we employed a bacterially expressed, active EphA4 kinase fragment to phosphorylate the Tyr604 and Tyr610 JMS sites in the EphB2 JMS-KD construct (see Supplementary data for details). As such, the resultant EphB2 active state differed from the reference auto-inhibited state only by the phosphorylation status of the JMS. Phosphorylation of Tyr604 and Tyr610 induced large spectral perturbations within the KD (Figure 3C) very similar to those observed in the EphB2 KD analysis (Figure 3A and C and Supplementary Figure S6). As for the KD, resonances corresponding to the JMS were absent from positions observed in

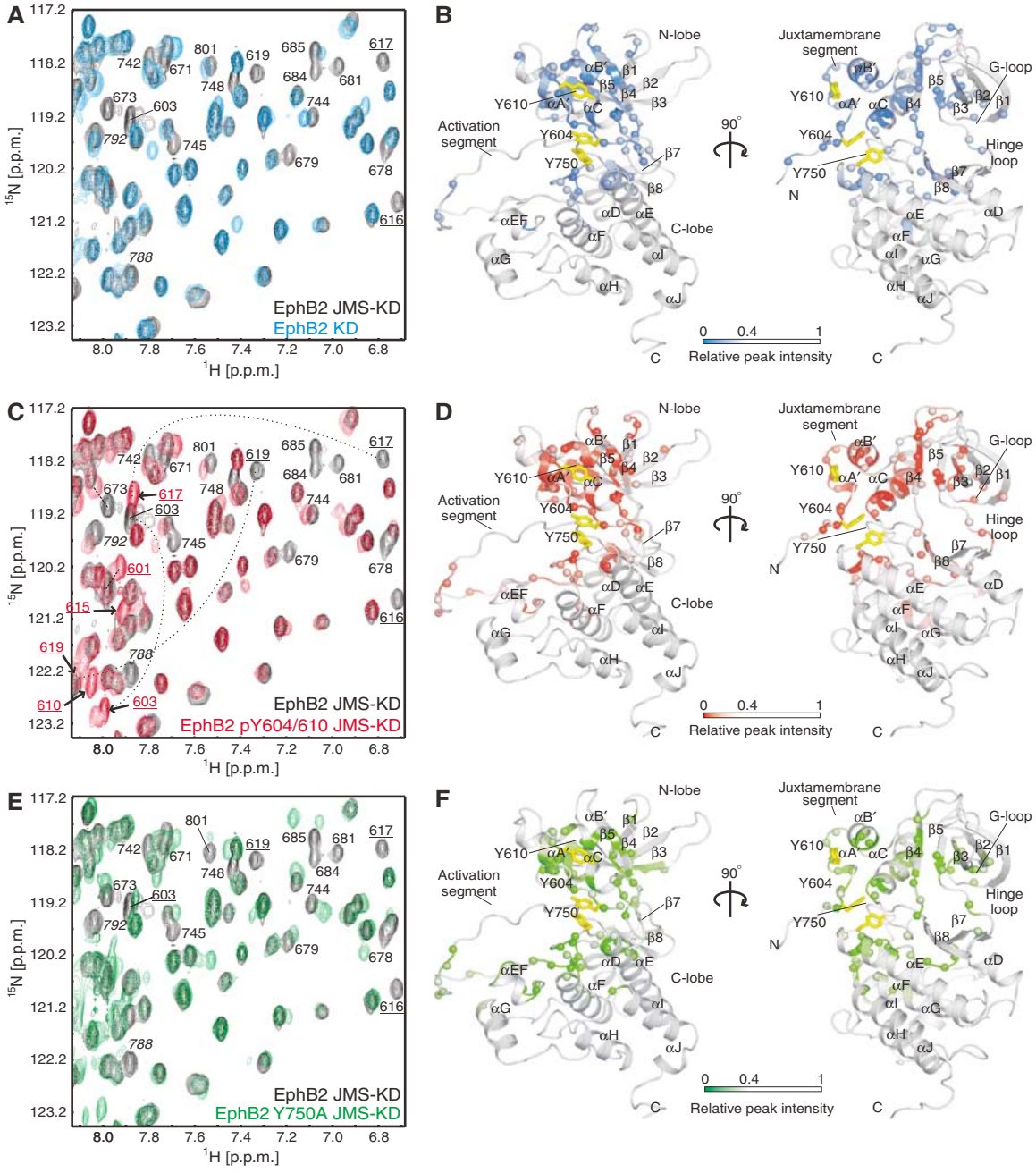

Figure 3 NMR spectral perturbation study of various activation states of EphB2 kinase. (**A**) Overlay of a representative region of the ^{1}H,^{15}N-HSQC spectra of the auto-inhibited EphB2 JMS-KD fragment (black) and the activated EphB2 KD fragment (blue). (**B**) Residues experiencing spectral perturbations are mapped onto the structure of the EphB2 JMS-KD as relative peak intensities with a linear gradient from white ($I/I_{ref} \geqslant 0.4$) to blue ($I/I_{ref} = 0$). Spheres represent the nitrogen atoms of affected residues. (**C**) As panel A, but for the EphB2 JMS-KD fragment phosphorylated on residues Y604 and Y610 (red). (**D**) As panel B, but for the phospho-JMS-KD fragment using a linear gradient from white to red. (**E**) As panel A, but for the EphB2 Y750A JMS-KD mutant (green). (**F**) As panel B, but for the EphB2 Y750A JMS-KD mutant using a linear gradient from white to green. In all spectral overlays, residues exhibiting significant spectral perturbations are labeled. JMS residues are underlined, whereas residues in the activation segment are in italics. Dotted lines indicate large chemical shift changes between the phosphorylated and unphosphorylated EphB2 JMS-KD fragment, whereas arrows highlight the positions of peaks appearing around 8.0 p.p.m. in the spectrum of the phosphorylated EphB2 JMS-KD.

the HSQC spectrum of the auto-inhibited state. However, sharp signals appeared around 8.0 p.p.m. in the HSQC spectrum of the active state (Figure 3C), a region in ^{1}H,^{15}N-HSQC spectra where amide protons of disordered residues are typically observed. Assignment of the $^{1}H^{N}$,^{13}C,^{15}N backbone resonances of the Tyr604/610 phosphorylated EphB2 JMS-KD (note that a full assignment was not performed for the two other active state EphB2 proteins studied herein) confirmed that the sharp resonances in the 8.0 p.p.m. region of the HSQC spectrum correspond to JMS residues (Figure 3C and Supplementary Figure S7). Furthermore, analysis of $^{13}C^{\alpha}$ and $^{13}C^{\beta}$ secondary chemical shifts (Supplementary Figure S5B) revealed that the phosphorylated JMS is disordered in solution. Thus, all NMR data are consistent with the JMS region

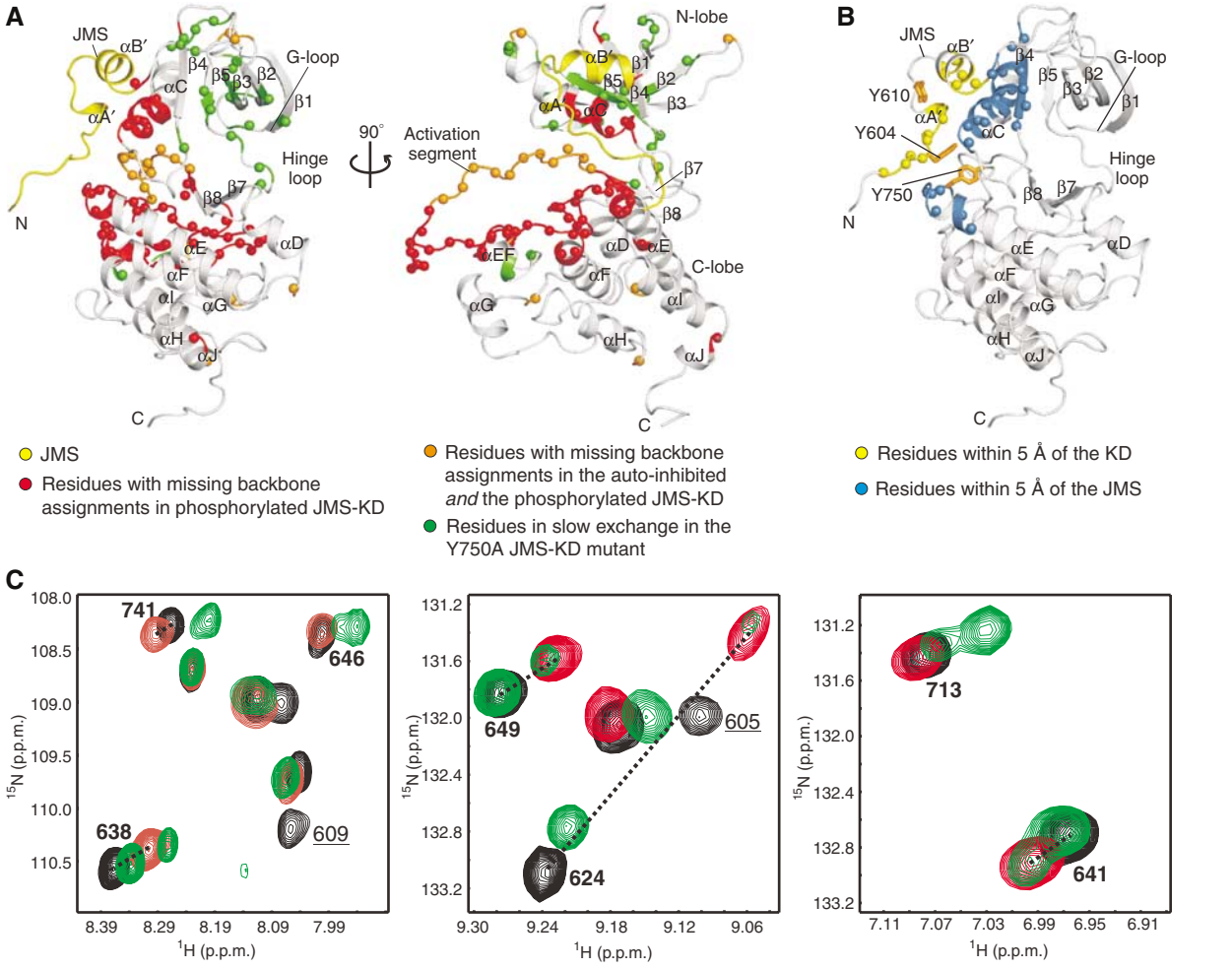

Figure 4 Activation of EphB2 kinase increases conformational dynamics within the KD. Evidence for inter-lobe motion based on increased line broadening in the active KD by comparison of the extent of backbone resonance assignments (**A**) in the auto-inhibited and phosphorylated, active EphB2 JMS-KD fragment. Residues in slow exchange (duplicated resonances) in the EphB2 Y750A JMS-KD mutant are also mapped onto the structure of the auto-inhibited EphB2 JM-KD fragment. Spheres represent nitrogen atoms affected by line broadening or peak duplication. (**B**) JMS-KD contacts mapped onto the structure of the auto-inhibited EphB2 JMS-KD fragment. Spheres represent nitrogen atoms in the JMS-KD binding surface. (**C**) Overlays of representative regions of the ^{1}H,^{15}N-HSQC spectra of the auto-inhibited EphB2 JMS-KD (black), the phospho-EphB2 JMS-KD (red) and the EphB2 Y750A JMS-KD mutant (green). Residues of the EphB2 Y750A JMS-KD mutant in slow exchange are labeled in bold, whereas JMS residues (605 and 609) are underlined. Dashed lines connect residues with large chemical shift changes upon phosphorylation.

transitioning from an ordered α-helical conformation to a disordered state in response to the phosphorylation of the JMS residues Tyr610 and Tyr604 (Supplementary Figure S5B and C).

As for the isolated EphB2 KD, large spectral perturbations were observed for numerous residues remote from the JMS contact site (Figure 3B and Supplementary Figures S6 and S7). With a full resonance assignment for the phosphorylated state in hand, we are able to distinguish whether low relative signal intensities at specific chemical shifts in the spectral perturbation studies are due to chemical shift changes, that is, relocation of particular resonances to different regions of the spectrum (indicating a stable conformational change), or are due to line broadening (indicating a change in protein dynamics toward the intermediate exchange regime typically corresponding to μs–ms timescale motions). Whereas backbone resonance assignments for the auto-inhibited JMS-KD fragment were >90% complete, those for the phosphorylated JMS-KD fragment were only 80% complete (Supplementary Figure S5A versus B), owing to more extensive line broadening in the active state spectra. Regions with incomplete resonance assignments in the phospho-JMS-KD include the C-terminal half of helix αC (aa 677–684), the catalytic loop (aa 745–758), the entire activation segment (aa 770–798) and the loop connecting helices αEF and αF (aa 807–815) (Figure 4A), providing evidence for a change in conformational dynamics for these regions. Interestingly, a majority of these residues map to the KD inter-lobe cleft, providing additional support to the notion that dissociation of the JMS increases inter-lobe flexibility (a possibility raised first by our X-ray structure analyses). Moreover, secondary chemical shifts for some residues in helix αC, the αC/β4-loop and the β4-strand differ more significantly from the auto-inhibited EphB2 JMS-KD than any other residue, apart from those of the JMS (Supplementary Figure S5C). Whereas helix αC adopts a single, ordered conformation in the auto-inhibited state, the active state NMR data reveal that the region encompassing helix αC undergoes conformational exchange between distinct states in response to JMS displacement.

As for the isolated KD, large chemical shift changes in the phospho-JMS-KD were observed for residues in the G-loop, the β3-strand and the hinge region (Figure 3B and D and Supplementary Figure S6). As these regions of the KD are remote from the JMS binding site, this result points toward indirect conformational rearrangements that may result from direct conformational changes in the vicinity of the inter-lobe cleft and/or helix αC.

The EphB2 Y750A JMS-KD mutant. The spectral perturbations observed for the $^{1}H,^{15}N$-correlation spectrum of the EphB2 Y750A JMS-KD mutant are qualitatively very similar to those observed for the EphB2 KD and the phospho-EphB2 JMS-KD (Figure 3E and F and Supplementary Figure S6). Most notably, the resonances of the JMS in the Y750A JMS-KD mutant are absent from their positions in the HSQC spectrum of the auto-inhibited JMS-KD. However, as for the phospho-JMS-KD, a number of resonance peaks appear with a proton chemical shift close to 8.0 p.p.m. (Figure 3E). Based on conclusions drawn from the assigned phospho-JMS-KD active state spectrum and the absence of visible electron density for the JMS in the EphA4 Tyr750Ala active state crystal structure, we interpret the appearance of resonances in the 8.0 p.p.m. region as an indication of JMS disorder in the Y750A mutant. Together with data indicating that the Y750A mutant bypasses a need for JMS phosphorylation, our results suggest that both phosphorylation of the JMS on Tyr604 and Tyr610 and mutation of Tyr750 to Ala cause the dissociation of the JMS from the KD.

Interestingly, the overlay of HSQC spectra for the auto-inhibited, the phospho-Tyr604/610 activated and the Tyr750Ala activated JMS-KD fragments shows that numerous KD residues of the Tyr750Ala mutant possess duplicated resonances and are thus in the slow exchange regime of the chemical shift (typically corresponding to millisecond and slower timescale motions). As shown in Figure 4C, duplicated resonance peaks in the Tyr750 mutant spectra coincide with assigned resonances in both active and auto-inhibited state spectra, reflecting an equilibrium between a higher populated inactive and a lower populated active state for most of the affected residues. Some of these duplicated resonances correspond to residues in the KD remote from the JMS binding site (Figure 4A and B), suggesting that JMS dissociation and KD activation propagate dynamic changes throughout almost the entire N-lobe. Although more experiments are needed to fully characterize the structural and dynamic basis of this phenomenon, our observations suggest that JMS phosphorylation is required in solution to fully shift the conformational equilibrium toward the active state.

In summary, our NMR results provide structural evidence that both the Y750A mutation and JMS phosphorylation induce dissociation of the JMS from the KD and its unfolding. In addition, our studies demonstrate that significant dynamic changes occur upon kinase activation within helix αC, the activation segment and the inter-lobe cleft, for which resonance broadening consistent with ms–μs timescale interconversions between distinct conformational states is evident. A change in conformational dynamics of the activation segment and orientational flexibility of helix αC with respect to the N-lobe β-sheet are in close agreement with the Eph receptor active state crystal structures.

Discussion

Mutation of Tyr750 to Ala in the C-lobe of the KD causes dissociation of the activation segment from the KD in a manner akin to phosphorylation of the JMS on residues Tyr604 and 610. This new activating mutation for the EphB2 and EphA4 RTKs is likely of general relevance to the whole Eph RTK family. The JMS dissociation event appears sufficient to activate catalytic function in part by allowing Tyr750 to adopt a conformation that no longer impedes the productive ordering of the activation segment. Although JMS displacement from the KD does not appear to be sufficient to lock the activation segment into a fixed productive conformation, it does allow a more productive conformation to be sampled in some of our X-ray crystal structures.

As evidenced by NMR, the resultant effects on KD structure arising from JMS dissociation by the Tyr750Ala KD mutation, phosphorylation of the JMS on Tyr604 and Tyr610, or deletion of the JMS are very similar, if not identical. Our X-ray structure analyses reveal that dissociation of the JMS from the KD leaves the characteristic kink in helix αC largely intact. This suggests that a highly populated, kinked helix αC is a general feature of all Eph receptor activation states. However, helix αC does in fact undergo detectable conformational exchange in solution in addition to being able to move with respect to the N-lobe β-sheet. If a change in the conformation of helix αC is relevant for regulating catalytic activity, then an important function of the JMS in the auto-inhibitory state may be to prevent a catalytically competent straight αC helix conformation from being sampled. In addition, conformational changes to helix αC could propagate structural changes to other parts of the N-lobe such as the G-loop, as suggested by our NMR data. In the auto-inhibited EphB2 crystal structure, a suboptimal orientation of the G-loop appeared to contribute to the inability of the KD to coordinate the sugar and phosphate groups of AMP-PNP.

Deletion of the JMS, introduction of the Tyr750Ala KD mutation and phosphorylation of the JMS all increase the catalytic function of the KD relative to a reference state, in which JMS phosphorylation is prevented. However, these experimental observations do not prove that the active states under investigation here correspond to the fully active form of the enzymes. Many protein kinases require activation segment phosphorylation for maximal activation and mutational analyses as well as conservation of Y^{act} (Tyr788) hint that this may also apply to Eph RTKs. However, in all our enzymatic studies, Y^{act} is not a detectable auto-phosphorylation site (Figure 1 and Supplementary Figure S3). One possible explanation for this observation is that the KD tyrosine sites are suboptimal auto-phosphorylation substrates relative to the JMS sites. Indeed, the efficient auto-phosphorylation sites Tyr604 and Tyr610 are embedded in a highly conserved sequence motif, YI/VDPxTYEDP (where x is any amino acid), that differs strikingly from the Y^{act} sequence (YTT/Sx). If Y^{act} is a suboptimal auto-phosphorylation site and yet serves a phosphoregulatory role, then phosphorylation of Y^{act} may be carried out by another protein kinase. In support of this notion, mutation of JMS tyrosines to glutamate renders the EphA4 kinase enzymatically more active *in vitro*, but still leaves it sensitive to receptor ligation *in vivo* (Egea *et al*, 2005). Potentially, receptor ligation facilitates phosphorylation of Y^{act} by a downstream kinase, for example,

Src or c-Abl (Kullander and Klein, 2002). If Y^{act} phosphorylation is necessary for full receptor activation, it will be very interesting to see what effect this modification has on the structure and dynamics of the KD.

KDs adopt strikingly similar, closed conformations in their active states, whereas the downregulated states of different protein kinases reveal a remarkable level of structural plasticity (Huse and Kuriyan, 2002). A common mechanism for regulating kinase activity involves preventing helix αC and the activation segment from attaining productive conformations. This is commonly achieved by intramolecular interactions with domains or polypeptide sequences that bind across the catalytic lobes (Huse and Kuriyan, 2002; Hubbard, 2004). A less considered consequence of these intramolecular interactions is the restriction of inter-lobe motion in the autoinhibited state. As most of our understanding of kinase function is based on static pictures from X-ray crystallography, residue-specific information about kinase dynamics in solution is still largely missing. Indeed, although distortion of helix αC and disorder of the activation segment persist even in the crystal structures of active Eph kinase states, our NMR analyses suggest that helix αC and the inter-lobe region undergo a significant change in conformational exchange upon kinase activation that propagates through almost the entire N-lobe of the KD. The two different views may reflect the fact that an X-ray structure is a snapshot of the most stable or a crystal favored conformation, which may be only one of many functionally relevant conformations sampled in solution. The idea of catalysis proceeding by dynamic fluctuations from a more stable conformation is consistent with the generally accepted theoretical understanding of enzymes as well as experimental observations, including a recent NMR dynamic study (Eisenmesser *et al*, 2005). In light of our NMR data, we posit that releasing the clamp imposed by intramolecular regulatory elements on inter-lobe orientation may be an important factor in kinase activation that is likely to be general to all Eph RTKs and other protein kinase families. More NMR studies on Eph RTKs as well as other kinases will allow us to understand this aspect of kinase regulation in more detail.

Materials and methods

Bacterial protein expression and purification

Eph RTK protein fragments used in enzymatic assays and crystallization trials were overexpressed as GST fusions and purified/cleaved as described (Wybenga-Groot *et al*, 2001). For NMR studies, His-tagged EphB2 fragments were expressed in *Escherichia coli* BL21(DE3) CodonPlus cells in 99.9% D_2O M9 minimal medium containing $^{15}NH_4Cl$ and $^{2}H,^{13}C$-glucose for $^{2}H,^{13}C,^{15}N$-labeled protein or in ~90% D_2O M9 minimal medium containing $^{15}NH_4Cl$ for $^{2}H,^{15}N$-labeled protein.

Mammalian protein expression, Western blotting and immunoprecipitation

EphA4 proteins transiently expressed in COS-1 cells were harvested as described previously (Holland *et al*, 1997; Binns *et al*, 2000). Proteins were resolved using 12% denaturing polyacrylamide gel electrophoresis (PAGE), transferred onto a polyvinylidene difluoride membrane (Millipore), blotted with anti-pTyr (Upstate Biotechnology) or anti-EphA4 antibodies (Park *et al*, 2004) and visualized using enhanced chemiluminescence (ECL Plus; Amersham).

Kinase assays

Kinetic analyses of bacterially expressed EphA4 JMS-KD fragments were performed using a coupled spectrophotometric kinase assay as described (Binns *et al*, 2000). *In vitro* kinase reactions using full-length EphA4 receptor immunoprecipitates or purified EphA4 fragments were performed as described previously (Park *et al*, 2004).

NMR methods

NMR data for resonance assignment were acquired at 25°C on a Varian Inova 600 MHz spectrometer for the JMS-KD fragment and at 500 MHz for the phospho-JMS-KD fragment. $^{1}H^{N},^{13}C$ and ^{15}N chemical shifts were assigned by standard methods (Sattler *et al*, 1999) using TROSY-based $^{1}H,^{15}N$-HSQC, HNCA, HN(CO)CA, HN(CA)CB, HN(COCA)CB, HNCO, HN(CA)CO experiments for the JMS-KD and phospho-JMS-KD fragment and a ^{15}N-edited NOESY ($t_{mix} = 100$ ms) recorded at 800 MHz for the JMS-KD fragment. All spectra were processed with the NMRPipe/NMRDraw package (Delaglio *et al*, 1995) and analyzed with XEASY (Bartels *et al*, 1995).

$^{1}H,^{15}N$-HSQC spectra for chemical shift mapping were recorded at 25°C on a Varian Inova 800 MHz spectrometer. Using the $^{1}H,^{15}N$ assignments of the EphB2-JMKD fragment, chemical shift perturbations were calculated with NMRDraw by dividing peak intensities in $^{1}H,^{15}N$-HSQC spectra of the auto-inhibited state (reference spectrum) and the respective active state spectrum (I/I_{ref}) at the exact positions of the peak maxima of the auto-inhibited state. Relative peak intensities were scaled for differences in sample concentrations and mapped onto the structure of the EphB2 JMS-KD (PDB ID 1JPA). Coordinates missing from the crystal structure were generated using the program MODELLERv7 (Sali and Blundell, 1993).

Supplementary data

Supplementary data are available at *The EMBO Journal* Online (http://www.embojournal.org).

Acknowledgements

We thank Gerry Gish for synthesis of S1 peptide, Lynne Howell for use of her diffractometer and Lewis Kay and Ranjith Muhandiram for invaluable assistance with NMR experiments. This work was supported by grants from the CIHR (FS and TP) and the National Cancer Institute of Canada (FS, TP and JDF-K). LEW-G was supported by a CIHR doctoral award, SW was supported by an Emmy Noether fellowship of the DFG and NW was supported by OGS and NSERC studentships. TP is a Distinguished Investigator of the CIHR.
Accession numbers: Atomic coordinates for the EphB2 KD and EphA4 Y604/610F, Y750A JMS-KD fragments were deposited in the Protein Data Bank under accession numbers 2HEN and 2HEL, respectively.

References

Bartels C, Xia T-H, Billeter M, Güntert P, Wüthrich K (1995) The program XEASY for computer-supported NMR spectral analysis of biological macromolecules. *J Biomol NMR* **5:** 1–10

Binns KL, Taylor PP, Sicheri F, Pawson T, Holland SJ (2000) Phosphorylation of tyrosine residues in the kinase domain and juxtamembrane region regulates the biological and catalytic activities of Eph receptors. *Mol Cell Biol* **20:** 4791–4805

Delaglio F, Grzesiek S, Vuister GW, Zhu G, Pfeifer J, Bax A (1995) NMRPipe: a multidimensional spectral processing system based on UNIX pipes. *J Biomol NMR* **6:** 277–293

Egea J, Nissen UV, Dufour A, Sahin M, Greer P, Kullander K, Mrsic-Flogel TD, Greenberg ME, Kiehn O, Vanderhaeghen P, Klein R (2005) Regulation of EphA4 kinase activity is required for a subset of axon guidance decisions suggesting a key role for receptor clustering in Eph function. *Neuron* **47:** 515–528

Eisenmesser EZ, Millet O, Labeikovsky W, Korzhnev DM, Wolf-Watz M, Bosco DA, Skalicky JJ, Kay LE, Kern D (2005) Intrinsic dynamics of an enzyme underlies catalysis. *Nature* **438:** 117–121

Ellis C, Kasmi F, Ganju P, Walls E, Panayotou G, Reith AD (1996) A juxtamembrane autophosphorylation site in the Eph family

receptor tyrosine kinase, Sek, mediates high affinity interaction with p59fyn. *Oncogene* **12:** 1727–1736

Eph Nomenclature Committee (1997) Unified nomenclature for the Eph family receptors and their ligands, the Ephrins. *Cell* **90:** 403–404

Hanks SK, Hunter T (1995) Protein kinases 6. The eukaryotic protein kinase superfamily: kinase (catalytic) domain structure and classification. *FASEB J* **9:** 576–596

Holland SJ, Gale NW, Gish GD, Roth RA, Songyang Z, Cantley LC, Henkemeyer M, Yancopoulos GD, Pawson T (1997) Juxtamembrane tyrosine residues couple the Eph family receptor EphB2/Nuk to specific SH2 domain proteins in neuronal cells. *EMBO J* **16:** 3877–3888

Hubbard SR (1997) Crystal structure of the activated insulin receptor tyrosine kinase in complex with peptide substrate and ATP analog. *EMBO J* **16:** 5572–5581

Hubbard SR (2004) Juxtamembrane autoinhibition in receptor tyrosine kinases. *Nat Rev Mol Cell Biol* **5:** 464–471

Huse M, Kuriyan J (2002) The conformational plasticity of protein kinases. *Cell* **109:** 275–282

Kalo MS, Pasquale EB (1999) Multiple *in vivo* tyrosine phosphorylation sites in EphB receptors. *Biochemistry* **38:** 14396–14408

Kullander K, Klein R (2002) Mechanisms and functions of Eph and ephrin signalling. *Nat Rev Mol Cell Biol* **3:** 475–486

Nolen B, Taylor S, Ghosh G (2004) Regulation of protein kinases; controlling activity through activation segment conformation. *Mol Cell* **15:** 661–675

Nowakowski J, Cronin CN, McRee DE, Knuth MW, Nelson CG, Pavletich NP, Rogers J, Sang BC, Scheibe DN, Swanson RV, Thompson DA (2002) Structures of the cancer-related Aurora-A, FAK, and EphA2 protein kinases from nanovolume crystallography. *Structure (Camb)* **10:** 1659–1667

Park EK, Warner N, Bong YS, Stapleton D, Maeda R, Pawson T, Daar IO (2004) Ectopic EphA4 receptor induces posterior protrusions via FGF signaling in *Xenopus* embryos. *Mol Biol Cell* **15:** 1647–1655

Sali A, Blundell TL (1993) Comparative protein modelling by satisfaction of spacial restraints. *J Mol Biol* **234:** 779–815

Sattler M, Schleucher J, Griesinger C (1999) Heteronuclear multidimensional NMR experiments for the structure determination of proteins in solution employing pulsed field gradients. *Prog NMR Spectrosc* **34:** 93–158

Wybenga-Groot LE, Baskin B, Ong SH, Tong J, Pawson T, Sicheri F (2001) Structural basis for autoinhibition of the EphB2 receptor tyrosine kinase by the unphosphorylated juxtamembrane region. *Cell* **106:** 745–757

Zisch AH, Kalo MS, Chong LD, Pasquale EB (1998) Complex formation between EphB2 and Src requires phosphorylation of tyrosine 611 in the EphB2 juxtamembrane region. *Oncogene* **16:** 2657–2670